Pressure and porosity influences on V_P-V_S ratio in unconsolidated sands

Mike Zimmer, Manika Prasad, and Gary Mavko, Stanford University, California, U.S.

Elevated pore pressures, commonly encountered in the shallow, unconsolidated section of the sedimentary column, present a significant hazard during the drilling and completion of offshore wells. The porosity of the ocean-floor sediments is high and a cover of low-permeability clay can prevent the underlying sediments from draining, even at very shallow depths below the seafloor. As further deposition loads the sediment, the entrapped fluids impede normal compaction by becoming pressurized. The lowered effective stress that results from the higher pore fluid pressure produces a proportional drop in the strength of non-cohesive sediments, resulting in very weak shallow sands. This weakness can result in washouts or fracturing in the shallow strata, potentially leading to the loss of the well and of neighboring wells.

These problems are exacerbated in deepwater wells where the long column of drill mud makes it difficult to control the pressure placed on the formation. In addition, slight overpressures result in a very narrow mud-weight window. A mud-weight below the pore pressure can result in shallow water flow, analogous to large scale washouts of unconsolidated sand layers. On the contrary, high mud weights can fracture these weak, shallow strata, with fractures potentially propagating all the way up to the surface and out to other wells in the same template (Ostermeier et al., 2000). The detection of high pore-pressure regions prior to drilling and the remote measurement of in-situ pressures has the potential to prevent the loss of many deepwater wells and of the millions of dollars that would be spent on them.

For a number of years, pore pressure evaluation has mainly relied on the use of empirical relationships between pressure and seismic velocities or interval transit times. Recently, Huffman and Castagna (2001) and Prasad (2002) have demonstrated the use of the V_P/V_S ratio as an indicator of pressure, as extracted from AVO analysis or multicomponent reflection data. One weak link in these analyses is the paucity of laboratory data available to calibrate the measured velocities or V_P/V_S to the in-situ pressure, especially for unconsolidated samples at the low effective pressures appropriate to this environment. This is in a large part due to the difficulties in propagating an ultrasonic signal through unconsolidated sediments at such low pressures. In an effort to constrain the velocity-pressure trends and to investigate the influence of porosity reduction on these trends, we have undertaken a systematic set of experiments to measure the ultrasonic velocities through loose sediments at effective pressures from below 100 kPa up to 20 MPa. Here we present measurements of *P*- and *S*-wave velocities through sand and glass bead samples at a range of porosities. We also discuss the effects of pressure, sorting, and compaction on the velocities and porosities, and implications for the evaluation of pore pressures using V_P/V_S in unconsolidated sands. This study did not include a number of other factors that could also influence the velocity-pressure relationship, including the age of the sediment, clay content, packing (or depositional environment), or stress-induced or inherent anisotropy, though they should be considered when attempting to predict in-situ pressure from velocity or V_P/V_S measurements.

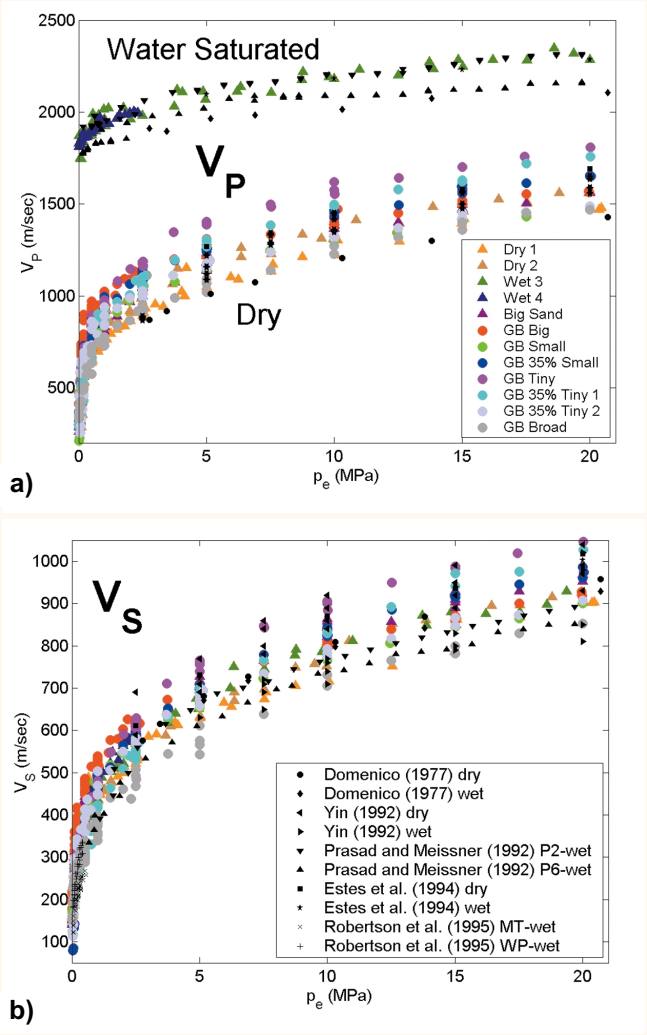

Figure 1. *P*- and *S*-wave velocity plotted against effective pressure for all of our sand and glass bead samples, and for similar measurements on clean sands from Prasad and Meissner (1992), Domenico (1977), Yin (1992), Estes et al. (1994), and Robertson et al. (1995).

Experimental methods and samples. We adapted a hydrostatic pressure apparatus to be able to make *P*- and *S*-wave velocity measurements on unconsolidated samples at low effective pressures. One adaptation was the use of lower frequency (200 kHz) transducers to produce and receive the ultrasonic signals. We also made the transducer face plates out of a glass-filled polycarbonate (shatterproof glass) in order to improve the acoustic impedance matching between the samples and the transducers. With this arrangement, we were able to get interpretable shear signals at pressures as low as 0.05 MPa, with errors of approximately 2% for *P*-wave velocities and 4% for *S*-wave velocities.

The data presented are from samples of a fine grained,

Table 1.

	Sample Name:	Initial Porosity				
Sands:	Dry 1	0.414	clean, quartz sand; well sorted			
	Dry 2	0.432	D_{10}=0.16 mm [1]			
	Wet 3	0.400	D_{60}=0.3 mm			
	Wet 4	0.411				
			Fraction	Size, μm (ϕ scale [2]	Fraction	Size, μm (ϕ scale)
	Big Sand	0.409	1	295-350 (1.5-1.75)	—	—
Glass Beads:						
	GB Big	0.381	1	295-350 (1.5-1.75)	—	—
	GB Small	0.411	1	74-88 (3.5-3.75)	—	—
	GB 35% Small	0.315	0.65	295-350 (1.5-1.75)	0.35	74-88 (3.5-3.75)
	GB Tiny	0.421	1	37-44 (4.5-4.75)	—	—
	GB 35% Tiny 1	0.296	0.65	295-350 (1.5-1.75)	0.35	37-44 (4.5-4.75)
	GB 35% Tiny 2	0.258	0.65	295-350 (1.5-1.75)	0.35	37-44 (4.5-4.75)
	GB Broad	0.338		37-710 (0.5-4.75)	—	—

[1] D_{10} and D_{60} are the grain diameters below which 10%, or 60% respectively, of the mass of the sample is found.

[2] $\phi = -\log_2 d$, where d is the grain diameter in mm.

well sorted, quartz sand called the Santa Cruz Aggregate, and from synthetic glass bead samples. Four samples of the Santa Cruz Aggregate were run, two dry (Dry 1, Dry 2) and two water-saturated (Wet 3, Wet 4). A fifth sample (Big Sand) was also prepared by sieving the 0.295-0.350 mm grain sizes out of this sand, and running this fraction dry. A total of seven glass bead samples were run, all dry. Three samples (GB Big, GB Small, and GB Tiny) consisted of different narrow size ranges of beads. Three samples (GB 35% Small, GB 35% Tiny 1 and 2) were made with a "bimodal" mixture of grain sizes, with 35% of the mass made up of smaller grains and 65% of larger grains. Finally, one sample (GB Broad) was made up of a broad range of particle sizes. Table 1 summarizes the grain sizes and initial porosities of all samples.

Special attention was given to preparing the samples in such a way as to ensure complete mixing of the different grain sizes, and to maintain full saturation of the water-saturated samples. However, the sample preparation varied based on whether the sample was a single grain size and dry (air pluviated) or water-saturated (water pluviated), or was a mixture of grain sizes (some samples mixed dry, some mixed while moist and allowed to dry once in the sample holder). These differences in sample preparation produced variations in the packing of the grains and some scatter in the data.

The porosity was calculated from the grain density, dry sample mass, and sample volume. The changes in the sample volume and porosity with pressure were then monitored by measuring changes in the length and circumference of the samples. The error in the porosity is estimated to be about 0.02, or about a 5% relative error.

The pressure path followed generally included a number of pressure cycles of increasing peak pressure for each cycle, up to 20 MPa. The velocities and porosity were measured at the same set of pressures during each cycle (e.g., 0.1, 0.2, 0.5... MPa). This allowed us to compare the velocities and porosities measured at the same pressure for a sample that had been preconsolidated to a range of higher pressures. Four samples were cycled through 8 cycles, while the rest were cycled through between 1 and 5 cycles.

Ultrasonic results. Figure 1 shows the *P*- and *S*-wave velocities plotted against pressure for all our samples, and for measurements on clean sands from Prasad and Meissner (1992), Domenico (1977), Yin (1992), Estes et al. (1994), and Robertson et al. (1995). This figure demonstrates similar trends between the data from all sources. The scatter is presumably a result of textural differences between the samples such as their sorting, angularity, packing (sample preparation), and mineralogy.

Figure 2a shows all of the dry velocity results plotted against porosity, and color-coded according to the effective pressure. The lower porosity data (below 0.35) come from the glass bead samples where two size fractions of beads were mixed, with the smaller grains partially filling the pore space between the larger grains. The lines in Figure 2a represent velocities calculated with the Reuss (isostress) average between the pure mineral moduli (quartz) and the high-porosity dry frame moduli for a given pressure. The high porosity end-member moduli come from the highest porosity data for each pressure, taken from the virgin compaction curve of sample Dry 2, which are highlighted with black circles in Figure 2a. The Reuss average, the weighted harmonic average between the two end member moduli, simulates the weakest possible way to combine two materials. Here the Reuss average is used to represent the minimum possible effect on the velocities of adding solid grain material (quartz) to the high porosity sample. The Reuss average was calculated as follows:

$$\frac{1}{M} = \frac{f_D}{M_D} + \frac{f_Q}{M_Q}$$

M is the resulting average modulus, M_D is the modulus of the dry frame at the pressure of interest, and M_Q is the modulus of pure quartz. The fraction of dry frame, f_D, is simply given by $f_D=\phi/\phi_0$, where ϕ is the porosity, and ϕ_0 is the initial porosity at that pressure from sample Dry 2. The fraction of pure quartz, f_Q is then just $1-f_D$, or $(1-\phi/\phi_0)$.

The data from a single sample (the streaks of points that rise more or less vertically in Figure 2a—e.g., the black or blue highlighted points) demonstrate the effect of the pressure on the velocity-porosity trend: a significant velocity increase with relatively little change in the porosity. Data collected at the same pressure, shown in the same color, illustrate the effects of sorting. Poorer sorting produces

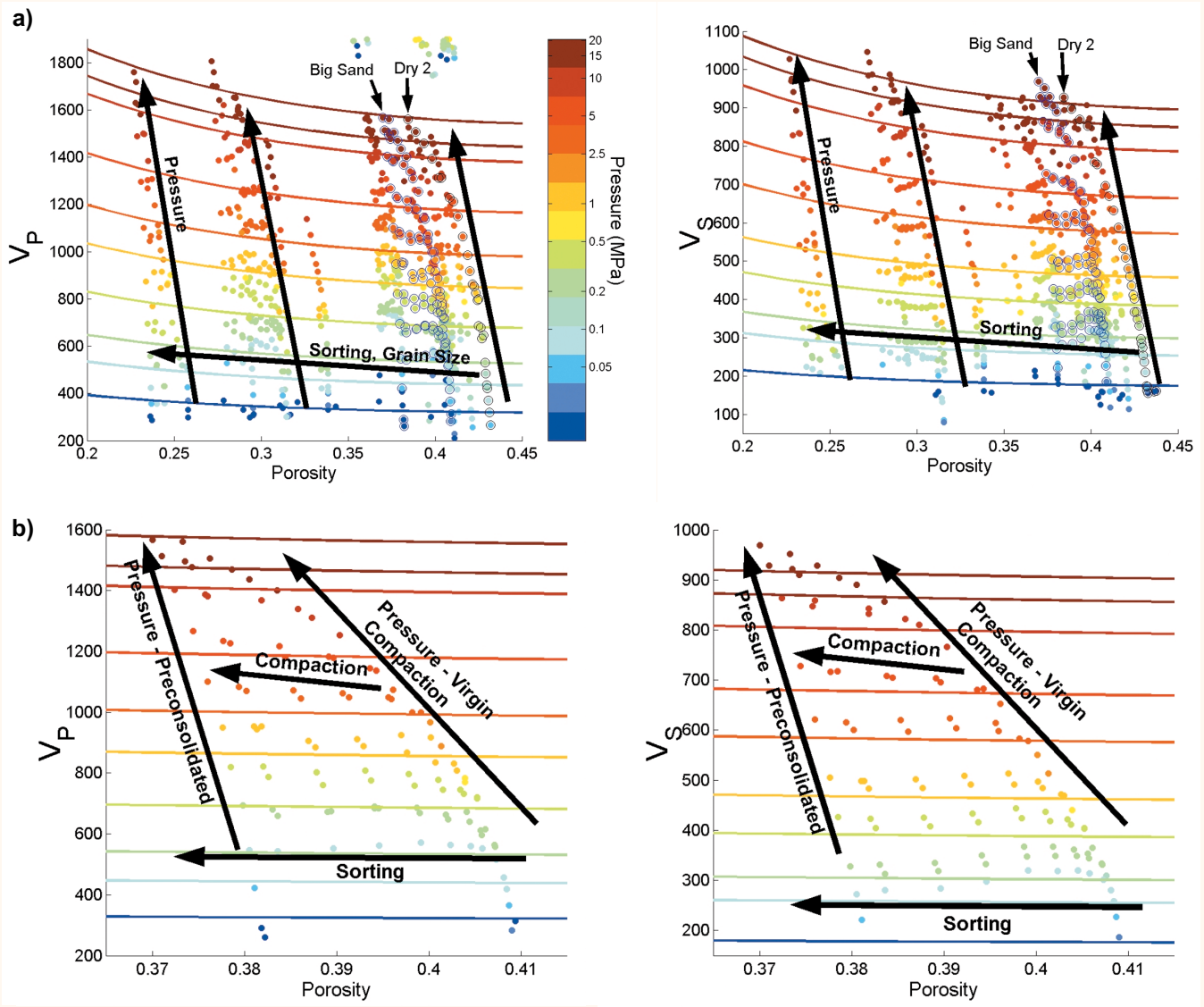

Figure 2. Velocity data plotted against porosity and color coded with effective pressure, along with lines showing the Reuss average between the quartz mineral modulus and the highest porosity dry-frame moduli for different pressures. The high porosity dry-frame moduli are taken from the virgin compaction curve of sample Dry 2, highlighted with black circles around the points. (a) All of the data. (b) Only data from the large size fraction sand (Big Sand), highlighted with blue circles in part (a), run dry through eight cycles of increasing peak pressure. The arrows indicate the effects on the velocity-porosity trend of pressure (for virgin loading and reloading of a preconsolidated sample), and of porosity reduction from changes in sorting or compaction.

large decreases in the porosity, but relatively small increases in the velocities. While there is some scatter in the data above and below the Reuss average, likely because these data come from glass bead and sand data prepared in slightly different ways, all in all the data collected at similar pressures do tend to lie along this trend. This result confirms the supposition of Dvorkin and Nur (1996) that the porosity variation produced by variations in sorting has a minimal (Reuss average) effect on the velocities. The implication is that the poorer sorting results in small grains lying passively in the pores between larger grains. Most small grains reduce the porosity but do not add significantly to the stiffness of the sediment, and so the velocity is only slightly increased.

Figure 2b illustrates the effect on the velocities of preconsolidation or compaction. This figure shows a velocity-porosity plot of the data from only the large size fraction sand, Big Sand, again color-coded by the pressure of the measurement. The data from this sample are highlighted with blue circles in Figure 2a. Also shown in Figure 2b are the same Reuss average lines as in Figure 2a, based on the virgin compaction curve of sample Dry 2. Sample Big Sand was run through eight pressure cycles, during which measurements were made at the same eight pressures for each cycle, once the peak pressure had exceeded that measurement pressure. Velocity measurements taken at the same pressure but compacted under higher preconsolidation pressures are seen to rise slightly as the porosity is reduced by compaction. This effect is more pronounced and more consistent for the higher measurement pressures. The rise is also slightly more pronounced for the *P*-wave velocities than for the *S*-wave velocities. For the higher measurement pressures, this effect is noticeably greater than the basically flat trend predicted by the Reuss averages based on the Dry 2 data. At the lower measurement pressures, the data follow the Reuss average trend fairly well, although the *S*-wave velocities rise slightly, then fall again with greater consolidation pressures.

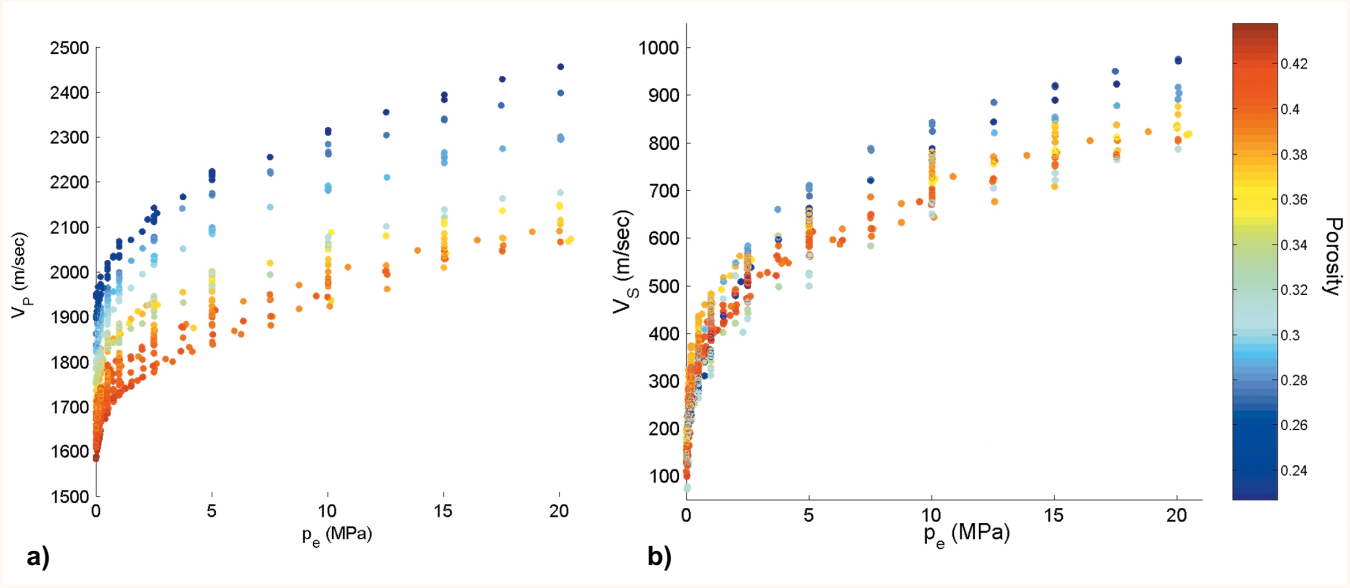

Figure 3. Velocity data from the glass bead samples plotted against effective pressure, and color coded according to porosity. (a) Gassmann fluid-substituted *P*-wave velocities. (b) Fluid(density)-substituted *S*-wave velocities. At low pressures the *P*-wave data still show a consistent porosity dependence, while the shear-wave velocities show less of a spread in the velocities at low pressure.

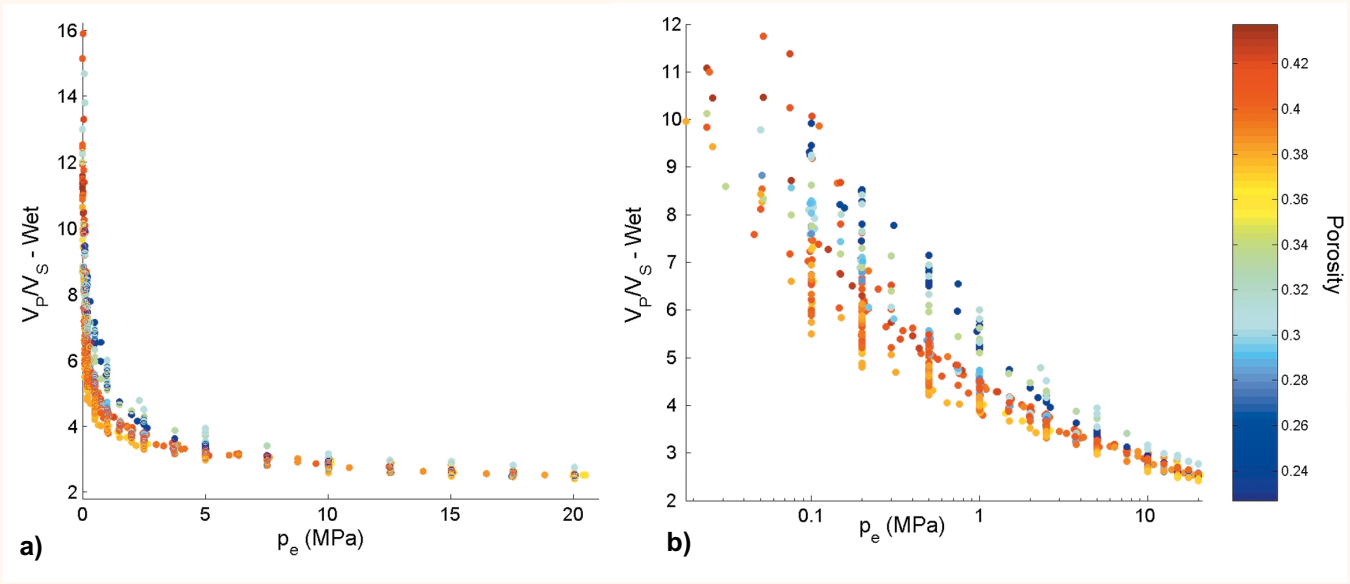

Figure 4. V_P/V_S ratio data for the water-saturated (Gassmann fluid-substituted) glass bead samples plotted against the effective pressure and color-coded for porosity. (a) Linear scale pressure-axis. (b) Log scale pressure-axis. The different porosity dependences of the water-saturated *P*- and *S*-wave velocities can be seen to produce a porosity dependence in the V_P/V_S ratio at low pressures.

Nevertheless, as for the case of sorting, the total effect on the velocities of this compaction-driven porosity reduction is relatively minor for these cohesionless sediments.

Figure 3 shows the results of Gassmann fluid substitution (with water) of the velocities of all the dry glass bead samples, plotted against pressure and color-coded for porosity. As seen in this figure, higher porosities produce lower *P*-wave velocities for the water-saturated samples. The shear-wave velocities, which require only a density substitution, show a similar porosity dependence at the higher pressures, with the low-porosity data resulting in higher velocities. At lower pressure, however, the porosity effect on the *S*-wave velocities is relatively small, as shown in the reduced scatter in Figure 3b and the rather flat Reuss average lines for the lower pressures in Figure 2a.

Pressure prediction. V_P/V_S ratios for all the Gassmann fluid-substituted glass bead data are shown in Figure 4, plotted against pressure and color-coded by porosity. As discussed by Prasad (2002) and Huffman and Castagna (2001), the water-saturated V_P/V_S shows a dramatic rise as the effective pressure decreases. The V_P/V_S ratio increases from below 3 at 10 MPa to a mean value of about 7 at 0.5 MPa. Unfortunately, at the lower pressures there is a considerable amount of scatter in the V_P/V_S ratio that would generate significant uncertainty in the in-situ effective pressure determined from V_P/V_S measurements. For example, if the measured V_P/V_S is 5, the in-situ pressure (based on our fluid-substituted glass bead data) could vary between 0.15 and 2 MPa.

In this study, we considered the effect of two factors

on the relationship between V_P/V_S and pressure: preconsolidation and sorting. Both factors influence the porosity of the sediment: preconsolidation by compaction of the grain matrix primarily through rearrangement of grains, and sorting by smaller grains filling pore spaces between larger grains.

Preconsolidation: Because these noncohesive sediments demonstrate only relatively small changes in both the velocity and porosity with compaction, we do not expect preconsolidation to produce a significant V_P/V_S signature. Preconsolidation does have a slightly larger effect on the dry *P*-wave velocities than on the *S*-wave velocities, as demonstrated in Figure 2b. At a given pressure, this would result in a slightly higher V_P/V_S in overconsolidated sediments than in normally consolidated ones. This effect does not persist once the data is fluid-substituted, which, except for some scatter at the very lowest pressures, shows no significant V_P/V_S signature from preconsolidation. So for water-saturated sands our results demonstrate no difference in V_P/V_S signature of overpressures produced through undercompaction or through repressurization mechanisms such as fluid expansion. As preconsolidation can cause a much larger reduction in the porosity of clay-rich sediments (Bowers, 1995; Sayers et al., 2001), this effect could potentially be important for cohesive sediments.

Sorting: At low pressures, the fluid-substituted V_P/V_S ratio is a function of both the pressure and the porosity, with low porosities corresponding to high V_P/V_S ratios (see Figure 4b). The porosity variation comes primarily from the differences in the initial porosities of the samples due to differences in their sorting. The spread in the V_P/V_S ratio comes from the different effects that the porosity has on the velocities, as demonstrated in Figure 3 and discussed above. As the relative porosity effect at high pressures is similar for the *P*- and *S*-wave velocities, there is relatively little scatter in V_P/V_S above about 10 MPa. The diminishing porosity-dependence of the *S*-wave velocities at lower pressures allows the porosity dependence of the *P*-wave velocity to show through. The implication is that for robust pressure estimates to be made from measured V_P/V_S, it will be necessary to correct for this porosity effect at pressures below about 10 MPa. Laboratory measurements on natural sands could potentially produce a relatively general porosity correction, but at present we would recommend cautious use of V_P/V_S as a quantitative pressure predictor.

Suggested reading. "Elastic properties of unconsolidated porous sand reservoirs" by Domenico (GEOPHYSICS, 1977). "Elasticity of high porosity sandstones: Theory for two North Sea data sets" by Dvorkin and Nur (GEOPHYSICS, 1996). "Overpressure detection from compressional- and shear-wave data" by Dvorkin et al. (*Geophysical Research Letters*, 1999). "The petrophysical basis for shallow-water flow prediction using mulitcomponent seismic data" by Huffman and Castagna (*TLE*, 2001). "Dealing with Shallow-Water Flow in the Deepwater Gulf of Mexico" by Ostermeier et al. (Proceedings - 32nd Offshore Technology Conference, 2000). "Acoustic measurements in sands at low effective pressure: Overpressure detection in sands" by Prasad, (GEOPHYSICS, 2002).

Acknowledgments: This work was supported by the Stanford Rock Physics and Borehole Geophysics Project and by the Department of Energy (under Award No. DE-FC26-01BC15354). The opinions, findings, conclusions, or recommendations expressed herein are those of the authors and do not necessarily reflect the views of the DOE. Gilbert Palafox provided invaluable assistance in designing the experimental apparatus.

Corresponding author: mzimmer@pangea.stanford.edu